NANO LETTERS
Letter
Cite This: Nano Lett. 2019, 19, 3440−3447
pubs.acs.org/NanoLett

Self-Sensing Enzyme-Powered Micromotors Equipped with pH-Responsive DNA Nanoswitches

Tania Patino,[§,&] Alessandro Porchetta,[∥,&] Anita Jannasch,[#] Anna Lladó,[‡] Tom Stumpp,[#] Erik Schäffer,[#] Francesco Ricci,[*,∥] and Samuel Sánchez[*,§,†]

[§]Institute for Bioengineering of Catalonia (IBEC), The Barcelona Institute of Science and Technology, Baldiri Reixac 10-12, Barcelona 08028, Spain

[†]Institució Catalana de Recerca i Estudis Avançats (ICREA), Pg. Lluís Companys 23, Barcelona 08010, Spain

[∥]Department of Chemistry, University of Rome, Tor Vergata, Via della Ricerca Scientifica 1, Rome 00133, Italy

[#]Center for Plant Molecular Biology (ZMBP), University of Tübingen, Auf der Morgenstelle 32, Tübingen 72076, Germany

[‡]Advanced Digital Microscopy, Institute for Research in Biomedicine (IRB Barcelona), The Barcelona Institute of Science and Technology, Barcelona 08010, Spain

S *Supporting Information*

ABSTRACT: Biocatalytic micro- and nanomotors have emerged as a new class of active matter self-propelled through enzymatic reactions. The incorporation of functional nanotools could enable the rational design of multifunctional micromotors for simultaneous real-time monitoring of their environment and activity. Herein, we report the combination of DNA nanotechnology and urease-powered micromotors as multifunctional tools able to swim, simultaneously sense the pH of their surrounding environment, and monitor their intrinsic activity. With this purpose, a FRET-labeled triplex DNA nanoswitch for pH sensing was immobilized onto the surface of mesoporous silica-based micromotors. During self-propulsion, urea decomposition and the subsequent release of ammonia led to a fast pH increase, which was detected by real-time monitoring of the FRET efficiency through confocal laser scanning microscopy at different time points (i.e., 30 s, 2 and 10 min). Furthermore, the analysis of speed, enzymatic activity, and propulsive force displayed a similar exponential decay, matching the trend observed for the FRET efficiency. These results illustrate the potential of using specific DNA nanoswitches not only for sensing the micromotors' surrounding microenvironment but also as an indicator of the micromotor activity status, which may aid to the understanding of their performance in different media and in different applications.

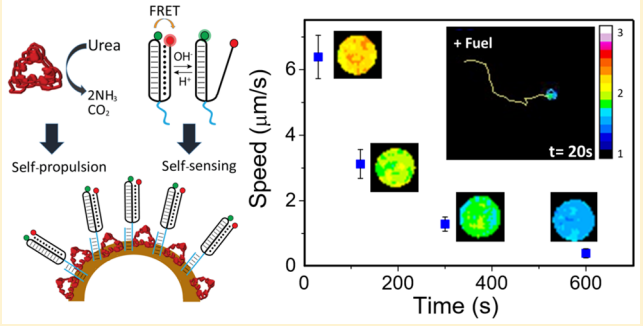

KEYWORDS: *Micromotors, DNA-nanoswitch, pH detection, self-propulsion, nanosensors, nanomotors*

Biological systems have developed complex mechanisms to regulate a number of activities, such as sensing, active transport, and motion control, through the integration of molecular-scaled biological motors and structure-switching elements. The creation of artificial machines able to mimic such complex biological functions could address several unmet challenges and open new research routes in nanotechnology.[1,2] As an example, several milestones have been achieved so far in this direction, such as the fabrication of micro- and nanomachines able to self-propel and perform complex tasks including cargo transport,[3−5] drug delivery,[6,7] or environmental remediation.[8−11]

In the past years, the quest for biocompatible systems with a high versatility of substrates has led to the development of biocatalytic motors that use enzymatic reactions to propel micro- and nanoparticles.[12−32] A step forward in the field would be to combine such devices with responsive biomolecules to provide multiple and simultaneous functionalities such as target recognition, imaging, or sensing capabilities. It is worth noting that to date biosensing applications of nano/micromotors have been much less exploited than those involving cargo delivery. A few examples of catalytic microswimmers for sensing purposes have been reported, where changes in speed or fluorescence were correlated to the presence of the target or analyte to be detected.[32−39] Sensing using enzyme-powered micromotors has been mainly reported for tubular microjets, where analytes modify the dynamics inhibiting the motion of micromotors.[40] Therefore, a method that allows a precise and quantitative sensing and at the same time can monitor chemical reactions is yet to be explored. In this regard, enzyme-powered micromotors modified with responsive biological receptors could

Received: November 30, 2018
Revised: January 28, 2019
Published: February 1, 2019

DOI: 10.1021/acs.nanolett.8b04794
Nano Lett. 2019, 19, 3440−3447

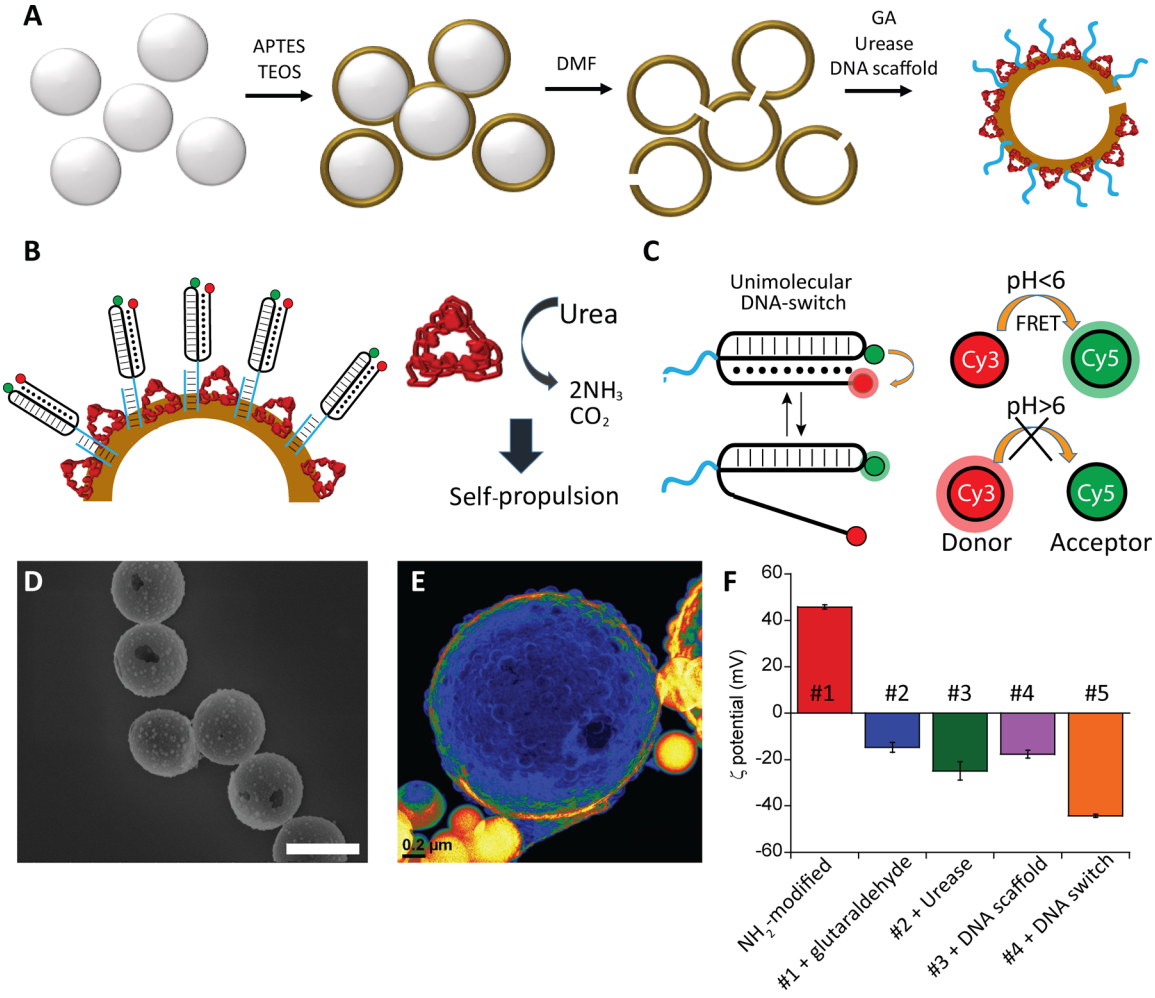

Figure 1. Fabrication approach and characterization of DNA micromotors. (A) Schematic representation of the micromotors fabrication, where a silicon dioxide layer is grown onto a commercial polystyrene template by adding APTES and TEOS silica precursors. The polystyrene core is then removed by DMF, and the microcapsules are functionalized with urease and a DNA strand (DNAss, blue) using glutaraldehyde (GA). (B) The pH-responsive DNA nanoswitch hybridizes to the complementary DNA scaffold that is covalently linked on the micromotor. Self-propulsion is achieved by the conversion of urea into ammonia and carbon dioxide, mediated by urease enzyme (red triangles). (C) The pH-dependent triplex-to-duplex transition of the unimolecular DNA nanoswitch results in a change of the FRET efficiency. (D) Scanning electron micrograph of SiO_2 microcapsules, prior to their functionalization. Inset shows a magnification of the selected area. Scale bar = 2 μm. (E) Topographical image obtained by transmission electron microscopy. Calibration bar indicates the height in μm. (F) ζ-potential measurements of the microparticle surface along the functionalization process.

offer an alternative for the analysis of their intrinsic activity and motion. In fact, the real-time monitoring of the responsive biomolecule in the presence of a specific chemical cue produced by the enzyme can provide a means to correlate the micromotor motion and activity (i.e., the enzymatic reaction).

To achieve this objective, the programmability of Watson–Crick interactions, the biocompability, and the unique ability of nucleic acid strands to respond to a plethora of different biological and chemical inputs could prove useful to perform sensing during motion. In particular, DNA-based nanodevices, which have been demonstrated for sensing and drug-delivery applications,[41,42] appear as perfect candidates to be integrated within synthetic motors. In analogy to cellular machines, synthetic DNA nanodevices can be rationally engineered and designed to be responsive to a molecular or chemical cue and are able to function in complex media.[43−45] Most of these artificially designed DNA nanodevices make use of structure-switching mechanisms to signal the presence of the specific input. As an example, a number of pH-responsive DNA-based conformational changing probes (nanoswitches) exploiting pH-dependent DNA triplex-forming interactions have been recently demonstrated as convenient pH nanosensors and programmable nanomachines for drug release applications.[46−50]

Here, we combine biocompatible enzymatic micromotors with DNA-based nanoswitches to fabricate multifunctional active devices able to move and continuously monitor the surrounding microenvironment. We functionalized enzyme-powered hollow silica microcapsules (i.e., urease-powered micromotors) that move in the presence of a specific substrate (urea) and modified them with a FRET-labeled pH-responsive DNA nanoswitch that allows us to instantaneously monitor pH changes of the solution caused by the enzymatic reaction responsible for micromotors self-propulsion.

Hollow silica microcapsules with amine groups on the surface were synthesized according to a previously reported co-condensation method,[14] based on the growth of a SiO_2 shell

DOI: 10.1021/acs.nanolett.8b04794
Nano Lett. 2019, 19, 3440−3447

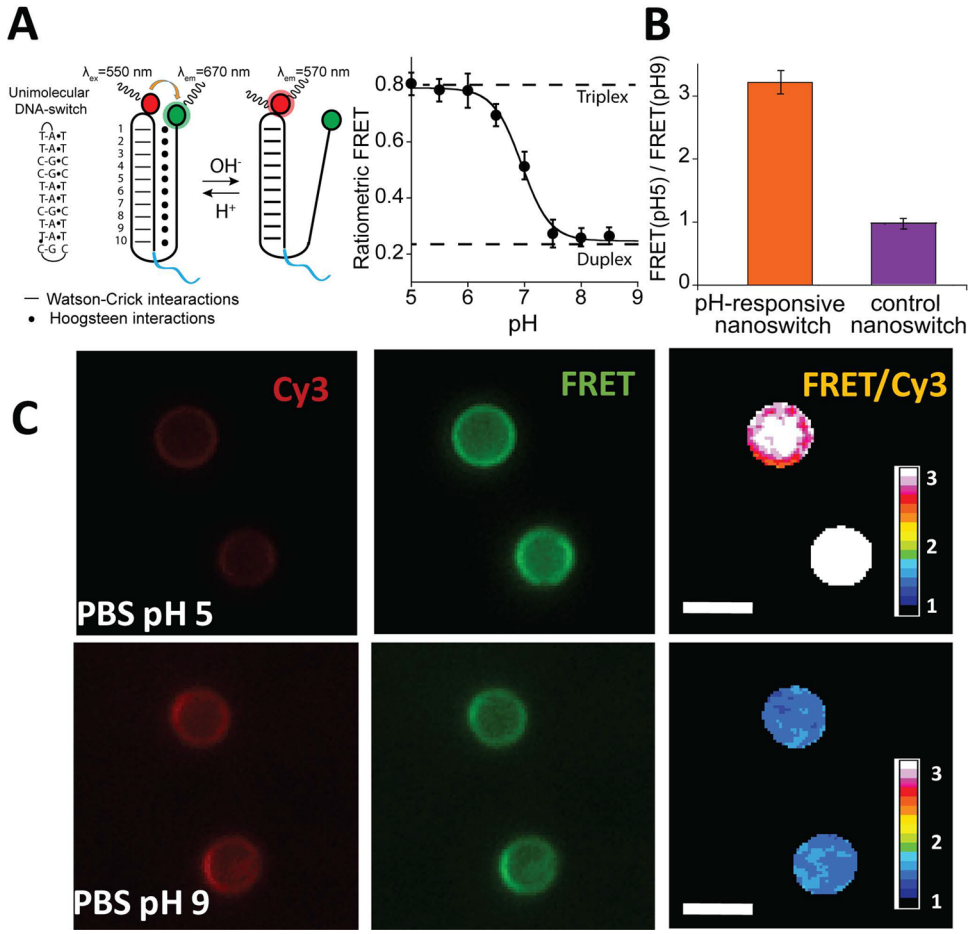

Figure 2. Triplex-based pH-responsive DNA nanoswitches are able to detect pH changes when conjugated to the micromotor structure. (A) Triplex DNA nanoswitch forms an intramolecular double hairpin structure through the formation of pH-insensitive Watson−Crick interactions (dashed line) and pH-sensitive Hoogsteen interactions (dots). Triplex nanoswitch containing CGC and TAT triplets unfolds into a duplex conformation at a basic pH. Ratiometric FRET emission plot shows the triplex-to-duplex transition of the DNA nanoswitch as a function of pH changes in solution. (B) FRET efficiency ratio between pH 5.0 and pH 9.0 for the triplex DNA nanoswitch and the control DNA nanoswitch (i.e., pH-independent). Here, the control DNA switch has the same intramolecular hairpin structure (WC interactions) and a random flanking tail that does not permit the triplex folding. (C) CSLM analysis of FRET effect of DNA nanoswitch-functionalized microparticles at pH 5.0 and 9.0, showing from right to left the Cy3 channel, FRET channel, and the FRET/Cy3 ratio value indicated in the calibration bar. Scale bar = 2 μm.

onto 2 μm diameter commercial polystyrene microparticles using 3-aminopropyltriethoxysilane (APTES) and tetraethylorthosilicate (TEOS) as silica precursors, followed by the removal of the polystyrene core by dimethylformamide, as depicted in Figure 1A. Urease was covalently conjugated to the micromotor surface using glutaraldehyde (GA) as a linker as previously described.[18,51] During this step, we also conjugated an amino-modified single-stranded DNA (DNAss, 20 bases) that served as the anchoring moiety for the pH-responsive DNA nanoswitch (Figure 1B). Figure 1C shows a schematic representation of the pH sensing strategy based on the open/closed states of the DNA-nanoswitch, which causes a high or low FRET efficiency, respectively. The resulting hollow microcapsules were studied by both scanning and transmission electron microscopy (SEM and TEM, respectively). Figure 1D shows a SEM micrograph where microcapsules with a very monodispersed size (2.04 ± 0.06 μm, mean ± standard error of the mean (N = 50)) and a rough surface can be observed. The microcapsules displayed a hole on their surface, probably due to the proximity of particles during the growth of the silica shell, as reported before, which provides a structural asymmetry.[51] Figure 1E shows a topographical image obtained by TEM, where the different pseudocolors indicate the height, in μm. The functionalization process was characterized by measuring the ζ-potential of microparticles after each step (Figure 1F). First, the microcapsules displayed a positively charged surface due to the presence of amine groups, which was then shifted to negatively charged due to the modification with GA. After urease addition, surface charges were slightly reduced. The functionalization with both urease and DNAss also resulted in a decrease of ζ -potential with respect to GA. Finally, microparticles were incubated in phosphate buffered saline (PBS) containing the DNA nanoswitch (i.e., 1 μM). A 15 min incubation of the nanoswitch with the enzyme/anchoring strand conjugated motors was sufficient to functionalize silica particles with the pH-responsive nanoswitch (Figure 1B,C). Of note, the switch presents a 20-base-long flanking tail (blue portion, Figure 2A) at the 5′-end of the sequence complementary to the DNAss covalently conjugated onto the silica microcapsule. As a result of the conjugation, a further decrease of the surface charges has been measured and confirms the effective functionalization of the motor with the switch.

DOI: 10.1021/acs.nanolett.8b04794
Nano Lett. 2019, 19, 3440−3447

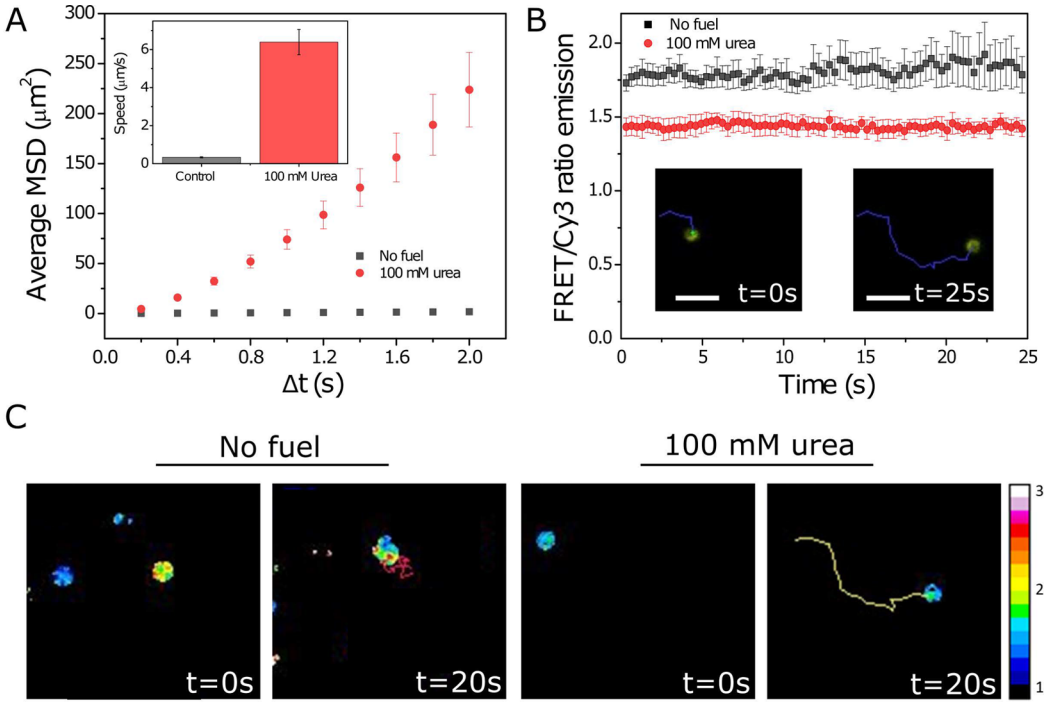

Figure 3. Motion dynamics and simultaneous FRET monitoring of DNA-modified urease micromotors. (A) Average MSD of DNA nanoswitch-modified micromotors in the presence/absence of fuel. Inset shows the speed, calculated from the MSD. Results are shown as the mean ± standard error of the mean (N = 20). (B) Real-time monitoring of the FRET/Cy3 ratio by CSLM recording of micromotors in the presence (100 mM) and in the absence of urea. Inset shows two different snapshots of the merged image obtained from FRET and Cy3 channels, at different time points (t = 5 and 25 s). Scale bar = 4 μm. (C) Snapshots of FRET/Cy3 recording at different time points in the absence or presence of urea (100 mM).

It is also noteworthy that our pH-responsive DNA nanoswitch is a triplex-forming single-stranded DNA containing an intramolecular DNA hairpin stabilized with both Watson−Crick and parallel Hoogsteen interactions. While the Watson−Crick (WC) interactions are effectively insensitive to pH, the Hoogsteen interactions show a strong and programmable pH dependence (Figure 2A).[49] By labeling the nanoswitch with a FRET pair, it is possible to monitor the pH-dependent triplex-to-duplex transition. This transition can be used to determine the pH of the solution in the vicinity of the micromotors. More specifically, a cyanine-3 fluorophore (Cy3) is internally conjugated in the loop of the hairpin duplex DNA, and a cyanine-5 fluorophore (Cy5) is linked at the 3′- end of the triplex-forming DNA portion. Fluorescence assays performed at a fixed concentration (i.e., 50 nM) of the DNA switch by varying the pH of the buffer solution in a fluorescence microcuvette (100 μL PBS solution) clearly demonstrate changes in the FRET efficiency as a function of pH (Figure S1). As expected, at acidic pH values, the intramolecular triplex structure is favored, and we observe a high FRET efficiency (Cy3 and Cy5 are brought in close proximity). As we increase the pH of the solution, the triplex structure is destabilized, and we observe a gradual decrease of the FRET signal due to the triplex-to-duplex transition (unfolding) (Figure 2A). Unlike other pH-responsive nanoprobes, our FRET-based DNA nanoswitch is thus a ratiometric probe that allows quantitative pH detection. Of note, fluorophores employed here are not responsive to pH changes in the range of investigation (from pH 5.0 to pH 9.5). It is also important to note that this class of triplex-based switches show opening/closing kinetics sufficiently fast to allow the real-time monitoring of pH variation (average time constant ∼100 ms) that occurs on longer time scales.[49] These unique features represent a crucial step forward to their implementation as real-time pH sensors in complex cellular environments.

To test the functionality of the switch once conjugated to the micromotors, FRET efficiency was monitored through a Leica-SP5 confocal laser scanning microscope (CSLM) equipped with a 63× oil immersion objective (Figure 2C). For this, micromotors were suspended in PBS either at pH 5.0 or pH 9.0 and placed in an 8-well glass-bottom dish for their analysis under CSLM. The emission of the donor (Cy3) was recorded using a 564 nm diode laser. The FRET image was obtained by exciting the Cy3 fluorophore and detecting the acceptor (Cy5) emission. Using a custom-made ImageJ plug-in,[52] we were able to quantify the FRET efficiency by calculating the FRET/Cy3 ratio where FRET and Cy3 are the total Cy5 (i.e., acceptor) and Cy3 (i.e., donor) fluorescence intensities, respectively, both following Cy3 excitation. These results indicate that the DNA-nanoswitch-modified micromotors were able to detect pH changes in their surrounding environment. To demonstrate the specificity of pH detection and discard any effect of the pH in the fluorescence intensity, we modified the micromotors with a control switch, which did not respond to pH changes (Figure S2). Figure 2B shows the quantification of FRET/Cy3 emission from micromotors modified with either a pH-responsive DNA-nanoswitch or a non-pH-responsive DNA nanoswitch (Figure 2B). Specifically, as a non-pH-responsive probe, we selected a single-stranded DNA containing the same intramolecular DNA hairpin stabilized through WC interactions and a scramble DNA tail that does not allow triplex folding. As expected, no significant differences were found when using the non-pH-responsive nanoswitch presenting a high FRET efficiency at all pH values evaluated as the switch remains in its closed state and the two fluorophores in tight contact.

DOI: 10.1021/acs.nanolett.8b04794
Nano Lett. 2019, 19, 3440−3447

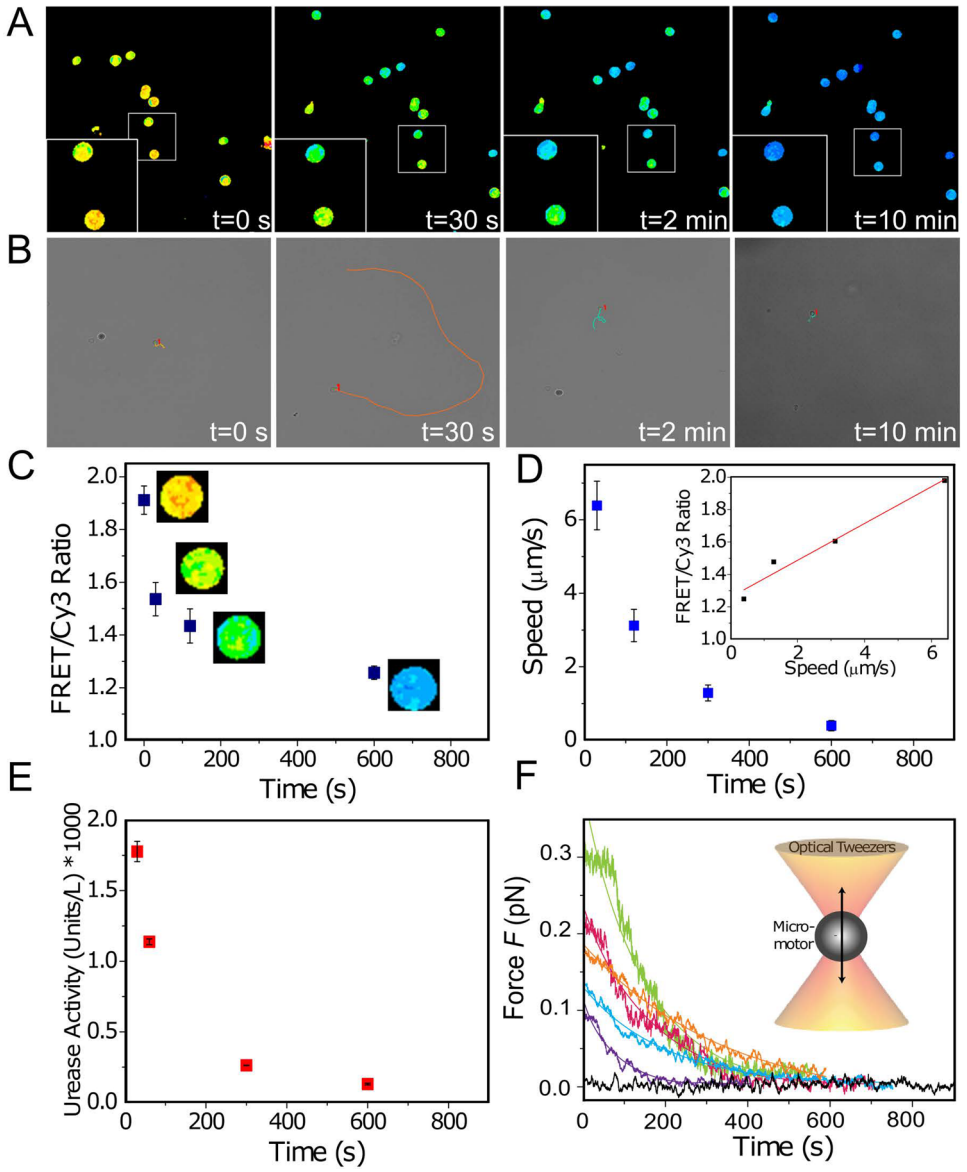

Figure 4. Self-sensing of micromotors activity through pH-responsive DNA nanoswitches and FRET imaging. (A) FRET/Cy3 ratio images of immobilized micromotors at the indicated time points after the addition of urea (100 mM). (B) Snapshots from the optical recording of micromotors trajectories (10 s) at the indicated time points after the addition of urea (100 mM). (C) FRET/Cy3 ratio of the micromotors incubated with urea (100 mM) at different time points. (D) Micromotors speed. Inset shows the correlation between speed and FRET/Cy3 ratio. (E) Enzymatic activity of micromotors overtime. (F) Propulsive force overtime measured by optical tweezers. Shown are force-time traces of single micromotors with 100 mM urea (colored lines) and without fuel (black line). The force-time traces for micromotors with fuel are fitted with an exponential decay function. Results are shown as the mean ± standard error of the mean.

The motion dynamics of hollow micromotors double functionalized with urease and DNA-nanoswitches was analyzed by optical microscopy either in the absence or presence of 100 mM urea acting as fuel, as previously reported.[18] To this end, we used a Leica DMi8 inverted fluorescence microscope equipped with a 63× water immersion objective and a C11440 Hamamatsu digital camera. At least 15 microparticles per condition were recorded during 25 s at a rate of 25 frames per second (FPS) (Videos S1 and S2). Using a Python-based code, the trajectories of the micromotors were tracked, and from the trajectories, the mean squared displacements (MSDs) were calculated according to eq 1:

$$\mathrm{MSD}\ (\Delta t) = \langle (x_i(t + \Delta t) - x_i(t))^2 \rangle \quad (1)$$

Figure 3A shows the average MSDs of micromotors as a function of the time interval (Δt). Upon addition of a urea substrate, the MSD showed a parabolic shape, which corresponds to a propulsive regime of an active microparticle.[53] However, in the absence of fuel, only Brownian motion was observed resulting in a liner fit. Together the data indicates that the motion arose from the catalytic reaction on the surface of the micromotors. The speed of propulsive particles (Figure 3A, inset) was found to be 6.4 ± 0.6 μm/s (mean ± standard error of the mean), calculated by using eq 2:

$$\mathrm{MSD}\ (t) = 4D_t t + v^2 t^2 \quad (2)$$

where D_t = diffusion coefficient, v = speed, and t = time.

DOI: 10.1021/acs.nanolett.8b04794
Nano Lett. 2019, 19, 3440−3447

This speed is comparable to asymmetric Janus enzyme-powered microcapsules reported by our group[18] and slightly higher than non-Janus microparticles.[51]

A recent work by Hess and co-workers reported that controlling and engineering the pH microenvironment on enzyme reactions increases the throughput and optimal efficiency.[54] The capability of micromotors to simultaneously record local pH changes produced while they are self-propelling was assessed by combining both optical tracking and FRET imaging using CSLM (Videos S3 and S4). In this case, having to record both Cy3 and FRET channels, we obtained a maximum time resolution of 3FPS. Figure 3B shows the results of the FRET/Cy3 ratio in the presence or absence of urea, recorded during 25 s. In the absence of fuel, a mean FRET/Cy3 ratio of 1.80 ± 0.09 or 1.8 ± 0.1 according with the sensitivity of your method (mean ± standard error of the mean) was observed. When urea was added to the solution, the FRET/Cy3 ratio immediately decreased to 1.50 ± 0.05, indicating a pH increase due to micromotors activity. No significant differences on the FRET/Cy3 ratio were observed during the 25 s of recording. Inset images show the FRET channel and the tracking trajectories of the micromotors at 5 s and 25 s. Figure 3C shows different snapshots of the real-time monitoring of micromotors in the presence (left) or absence (right) of fuel, showing the FRET/Cy3 ratio images at different time points (0 and 20 s). In the absence of fuel, the micromotors only displayed Brownian motion and a FRET/Cy3 ratio close to 2. By contrast, in the case of micromotors exposed to urea, the FRET/Cy3 ratio was already decreased at the moment of analysis (0 s). This indicates that the pH had already changed. This quick change is expected because the urease-based enzymatic reaction immediately takes place after adding a urea substrate, inducing a local pH change around the particles. These results demonstrate the capabilities of active DNA-modified micromotors to sense the microenvironment around them while producing a continuous chemical reaction for self-propulsion.

To gain insights into the instantaneous pH change around the micromotors from the initial moment of the reaction and be able to monitor the same particles along time, we immobilized micromotors onto a glass surface using APTES as a coating agent. APTES provided positive surface charges and led to stable electrostatic interactions with the negatively charged micromotors. Immobilizing micromotors allowed us to visualize the same micromotors prior and after the addition of fuel, as well as the analysis at longer time periods (2 and 10 min). Without immobilization, micromotors would move out the region of interest earlier. Figure 4A shows the FRET/Cy3 ratio images prior to (0 s) and after the addition of 100 mM urea to the immobilized micromotors at different time points (i.e., 30 s, 2 and 10 min). Before the addition of fuel, a high FRET/Cy3 ratio is observed with values above 2. Upon the addition of urea, a continuous decrease in the FRET/Cy3 ratio was observed for the different time points. The observed reduction in the FRET/Cy3 ratio can be explained by the local increase of pH induced by the production of ammonia upon urea decomposition by urease ($(NH_2)_2CO + H_2O \rightarrow CO_2 + 2NH_3$). Simultaneously, the motion dynamics was analyzed at the same time points by performing optical recordings of the micromotors for 30s at 25 FPS. Figure 4B shows different snapshots of the micromotors trajectories during 10 s, recorded at 30 s, and 2 and 10 min after the addition of fuel, where a significant decrease of the motion overtime can be observed. Since the DNA nanoswitch could measure local pH changes produced upon urease activity, we hypothesized that the FRET/Cy3 emission could be used as an indicator of the micromotors self-propulsion and activity. First, we quantified the FRET/Cy3 ratios at different time points, which showed a decrease overtime, indicating an increase in the pH of the surrounding microenvironment. Figure 4C shows the calculated FRET/Cy3 ratios at time 0, 30 s, 2 and 10 min, respectively, where the insets correspond to representative images of the indicated time points. A similar decrease as a function of time was observed when analyzing the speed of the micromotors (Figure 4D), where a positive correlation between the speed of the motors and the FRET/Cy3 ratio was observed, indicating a decrease in the speed while the pH increased (Figure 4D, inset). To elucidate whether the speed reduction was attributed to a lower enzymatic activity, urease activity was measured through a commercial kit (see the Supporting Information), which resulted in a similar trend to the one observed for the speed analysis (Figure 4E).

To confirm that the micromotor self-propulsion decreased over time in a nonlinear fashion, we measured the propulsion force of urease-powered PS@SiO_2 micromotors[18] as a function of time using high-resolution optical tweezers (Figure S3, Figure 4F).[55] To this end, we trapped single micromotors and measured their displacement from the trap center. Using the calibrated trap stiffness,[56,57] we calculated the propulsion force of urease-powered micromotors.[18] We observed that the propulsion force decreased exponentially over time with a half-life time constant of 123 ± 20 s (mean ± standard error of the mean, $N = 10$) (Figure 4F). Thus, all four measurements, FRET/Cy3 ratio, speed, enzymatic activity, and force, decreased overtime, following a similar trend. To understand whether the decrease in micromotors activity could be due to the pH increase upon the production of ammonia, we measured enzyme activity at pH 5, 6, 7, 8, and 9, where we observed a maximum activity at pH 6 and a significant activity decrease at pH 9 (Figure S4). Taken together, these results indicate that pH-responsive DNA nanoswitches could be used as self-sensing indicators, i.e., sensing their own activity over time.

Conclusions. We have demonstrated the potential of combining self-propelled biocatalytic micromotors with synthetic DNA nanodevices able to detect pH changes in the surrounding environment, which is used to monitor their activity profile. Urease-powered micromotors contain a double functionality as they can, at the same time, self-propel and sense pH changes through FRET imaging. Unlike other pH-responsive nanoprobes, our DNA nanoswitch is a photostable FRET-based sensor and a ratiometric probe, which allows quantitative pH detection within a few microseconds. Thanks to these features, our system represents a step forward to the real-time monitoring of microenvironment changes and of the intrinsic activity of the micromotors while swimming. Upon micromotors' activation in the presence of the enzymatic substrate, we observed a fast decrease in the FRET/Cy3 ratio, which was correlated with the speed, enzyme activity, and propulsive force. Future works should be devoted to increase the lifetime of enzyme-powered nanomicromotors, where the integration of self-sensing molecules could be useful to monitor their intrinsic activity to understand the changes in motion dynamics and their performance in different environments. In addition, the high versatility of DNA and enzymes

DOI: 10.1021/acs.nanolett.8b04794
Nano Lett. 2019, 19, 3440−3447

allows the tailoring of micromotors properties for a wide range of applications such as monitoring intracellular and intratissue pH or to monitor the pH of polluted water.

■ ASSOCIATED CONTENT

Supporting Information

The following files are available free of charge. The Supporting Information is available free of charge on the ACS Publications website at DOI: 10.1021/acs.nanolett.8b04794.

Raw fluorescence emission of the pH-dependent DNA nanoswitch at different pH's, confocal imaging of the micromotors functionalized with non-pH-responsive DNA nanoswitches at different pH's, optical trapping force F_{trap} in optical tweezers, and activity of urease-powered micromotors at different pH's (PDF)

Video S1 (AVI)

Video S2 (AVI)

Video S3 (AVI)

Video S4 (AVI)

■ AUTHOR INFORMATION

Corresponding Authors

*E-mail: francesco.ricci@uniroma2.it.

*E-mail: ssanchez@ibecbarcelona.

ORCID

Alessandro Porchetta: 0000-0002-4061-5574

Erik Schäffer: 0000-0001-7876-085X

Francesco Ricci: 0000-0003-4941-8646

Samuel Sánchez: 0000-0002-5845-8941

Author Contributions

&T.P. and A.P. contributed equally. S.S. and F.R. designed the project and initiated the idea. T.P. performed experiments on micromotors, tracking, and FRET imaging. A.P. performed nanoswitch characterization and supported the functionalization of motors. A.L. supported the experimental design for FRET imaging and data analysis. A.J., T.S., and E.S. performed the force measurement of micromotors using optical tweezers. T.P. and S.S. wrote the manuscript with input from F.R. and A.P. The manuscript was written through contributions of all authors. All authors have given approval to the final version of the manuscript.

Notes

The authors declare no competing financial interest.

■ ACKNOWLEDGMENTS

This work was supported by the European Research Council, ERC (project no. 336493, Nature Nanodevices) (F.R.), by Associazione Italiana per la Ricerca sul Cancro, AIRC (project no. 14420) (F.R.), the Spanish Ministry of Economy and Competitiveness, MINECO, through the projects CTQ2015-68879-R (MICRODIA) and CTQ2015-72471-EXP (Enzwim) (S.S.), the BBVA foundation (MEDIROBOTS) (S.S.), the CERCA Programme by the Generalitat de Catalunya (S.S.), and the University of Tübingen. T.P. thanks MINECO for the Juan de la Cierva fellowship. The authors thank A. M-López for developing the Python code for motion analysis.

■ REFERENCES

(1) De Ávila, B. E. F.; Angsantikul, P.; Ramírez-Herrera, D. E.; Soto, F.; Teymourian, H.; Zhang, L.; Wang, J. *Sci. Robot.* **2018**, *3*, No. eaat0485.

(2) Fischer, T.; Agarwal, A.; Hess, H. *Nat. Nanotechnol.* **2009**, *4*, 162−166.

(3) Baylis, J. R.; Yeon, J. H.; Thomson, M. H.; Kazerooni, A.; Wang, X.; St John, A. E.; Lim, E. B.; Chien, D.; Lee, A.; Zhang, J. Q.; Piret, J. M.; Machan, M. S.; Burke, T. F.; White, N. J.; Kastrup, C. J. *Sci. Adv.* **2015**, *1*, No. e1500379.

(4) Baraban, L.; Makarov, D.; Streubel, R.; Mönch, I.; Grimm, D.; Sanchez, S.; Schmidt, O. G. *ACS Nano* **2012**, *6*, 3383−3389.

(5) Sundararajan, S.; Lammert, P. E.; Zudans, A. W.; Crespi, V. H.; Sen, A. *Nano Lett.* **2008**, *8*, 1271−1276.

(6) Kagan, D.; Laocharoensuk, R.; Zimmerman, M.; Clawson, C.; Balasubramanian, S.; Kang, D.; Bishop, D.; Sattayasamitsathit, S.; Zhang, L.; Wang, J. *Small* **2010**, *6*, 2741−2747.

(7) Tu, Y.; Peng, F.; André, A. A. M.; Men, Y.; Srinivas, M.; Wilson, D. A. *ACS Nano* **2017**, *11*, 1957−1963.

(8) Gao, W.; Wang, J. *ACS Nano* **2014**, *8*, 3170−3180.

(9) Soler, L.; Sanchez, S. *Nanoscale* **2014**, *6*, 7175−7182.

(10) Soler, L.; Magdanz, V.; Fomin, V. M.; Sanchez, S.; Schmidt, O. G. *ACS Nano* **2013**, *7*, 9611−9620.

(11) Guix, M.; Orozco, J.; Garcia, M.; Gao, W.; Sattayasamitsathit, S.; Merkoci, A.; Escarpa, A.; Wang, J. *ACS Nano* **2012**, *6*, 4445−4451.

(12) Dey, K. K.; Zhao, X.; Tansi, B. M.; Méndez-Ortiz, W. J.; Córdova-Figueroa, U. M.; Golestanian, R.; Sen, A. *Nano Lett.* **2015**, *15*, 8311−8315.

(13) Ma, X.; Jannasch, A.; Albrecht, U.-R.; Hahn, K.; Miguel-López, A.; Schäffer, E.; Sánchez, S. *Nano Lett.* **2015**, *15*, 7043−7050.

(14) Ma, X.; Wang, X.; Hahn, K.; Sánchez, S. *ACS Nano* **2016**, *10*, 3597−3605.

(15) Ma, X.; Sánchez, S. *Tetrahedron* **2017**, *73*, 4883−4886.

(16) Ma, X.; Hortelao, A. C.; Miguel-López, A.; Sánchez, S. *J. Am. Chem. Soc.* **2016**, *138*, 13782−13785.

(17) Ma, X.; Hortelão, A. C.; Patiño, T.; Sánchez, S. *ACS Nano* **2016**, *10* (10), 9111−9122.

(18) Patiño, T.; Feiner-Gracia, N.; Arqué, X.; Miguel-López, A.; Jannasch, A.; Stumpp, T.; Schäffer, E.; Albertazzi, L.; Sánchez, S. *J. Am. Chem. Soc.* **2018**, *140*, 7896−7903.

(19) Patino, T.; Arqué, X.; Mestre, R.; Palacios, L.; Sánchez, S. *Acc. Chem. Res.* **2018**, *51*, 2662−2671.

(20) Joseph, A.; Contini, C.; Cecchin, D.; Nyberg, S.; Ruiz-Perez, L.; Gaitzsch, J.; Fullstone, G.; Tian, X.; Azizi, J.; Preston, J.; Volpe, G.; Battaglia, G. *Sci. Adv.* **2017**, *3*, e1700362.

(21) Mano, N.; Heller, A. *J. Am. Chem. Soc.* **2005**, *127*, 11574−11575.

(22) Pantarotto, D.; Browne, W. R.; Feringa, B. L. *Chem. Commun.* **2008**, *13*, 1533−1535.

(23) Sanchez, S.; Solovev, A. A.; Mei, Y.; Schmidt, O. G. *J. Am. Chem. Soc.* **2010**, *132*, 13144−13145.

(24) Sitt, A.; Soukupova, J.; Miller, D.; Verdi, D.; Zboril, R.; Hess, H.; Lahann, J. *Small* **2016**, *12*, 1432−1439.

(25) Gregory, D. A.; Zhang, Y.; Smith, P. J.; Zhao, X.; Ebbens, S. J. *Small* **2016**, *12*, 4048−4055.

(26) Abdelmohsen, L. K. E. A.; Nijemeisland, M.; Pawar, G. M.; Janssen, G.-J. A.; Nolte, R. J. M.; van Hest, J. C. M.; Wilson, D. A. *ACS Nano* **2016**, *10*, 2652−2660.

(27) Simmchen, J.; Baeza, A.; Ruiz, D.; Esplandiu, M. J.; Vallet-Regí, M. *Small* **2012**, *8*, 2053−2059.

(28) Simmchen, J.; Baeza, A.; Ruiz-Molina, D.; Vallet-Regí, M. *Nanoscale* **2014**, *6*, 8907−8913.

(29) Schattling, P. S.; Ramos-Docampo, M. A.; Salgueiriño, V.; Städler, B. *ACS Nano* **2017**, *11*, 3973−3983.

(30) Pavel, I.-A.; Bunea, A.-I.; David, S.; Gáspár, S. *ChemCatChem* **2014**, *6*, 866−872.

(31) Nijemeisland, M.; Abdelmohsen, L. K. E. A.; Huck, W. T. S.; Wilson, D. A.; van Hest, J. C. M. *ACS Cent. Sci.* **2016**, *2*, 843−849.

(32) Bunea, A.-I.; Pavel, I.-A.; David, S.; Gáspár, S. *Biosens. Bioelectron.* **2015**, *67*, 42−48.

(33) Parmar, J.; Vilela, D.; Villa, K.; Wang, J.; Sánchez, S. *J. Am. Chem. Soc.* **2018**, *140*, 9317−9331.

DOI: 10.1021/acs.nanolett.8b04794
Nano Lett. 2019, 19, 3440−3447

(34) Wu, J.; Balasubramanian, S.; Kagan, D.; Manesh, K. M.; Campuzano, S.; Wang, J. *Nat. Commun.* **2010**, *1*, 36.
(35) Campuzano, S.; Kagan, D.; Orozco, J.; Wang, J. *Analyst* **2011**, *136*, 4621−4630.
(36) Kagan, D.; Calvo-Marzal, P.; Balasubramanian, S.; Sattayasamitsathit, S.; Manesh, K. M.; Flechsig, G.-U.; Wang, J. *J. Am. Chem. Soc.* **2009**, *131*, 12082−12083.
(37) Molinero-Fernandez, A.; Moreno-Guzman, M.; Lopez, M. A.; Escarpa, A. *Anal. Chem.* **2017**, *89*, 10850−10857.
(38) Esteban-Fernandez de Avila, B.; Martín, A.; Soto, F.; Lopez-Ramirez, M. A.; Campuzano, S.; Vasquez-Machado, G. M.; Gao, W.; Zhang, L.; Wang, J. *ACS Nano* **2015**, *9*, 6756−6764.
(39) Karshalev, E.; Esteban-Fernández de Ávila, B.; Wang, J. *J. Am. Chem. Soc.* **2018**, *140*, 3810−3820.
(40) Orozco, J.; García-Gradilla, V.; D'Agostino, M.; Gao, W.; Cortés, A.; Wang, J. *ACS Nano* **2013**, *7*, 818−824.
(41) Harroun, S. G.; Prévost-Tremblay, C.; Lauzon, D.; Desrosiers, A.; Wang, X.; Pedro, L.; Vallée-Bélisle, A. *Nanoscale* **2018**, *10*, 4607−4641.
(42) Seeman, N. C.; Sleiman, H. F. *Nat. Rev. Mater.* **2017**, *3*, 17068.
(43) Porchetta, A.; Ippodrino, R.; Marini, B.; Caruso, A.; Caccuri, F.; Ricci, F. *J. Am. Chem. Soc.* **2018**, *140*, 947−953.
(44) Del Grosso, E.; Idili, A.; Porchetta, A.; Ricci, F. *Nanoscale* **2016**, *8*, 18057−18061.
(45) Porchetta, A.; Vallée-Bélisle, A.; Plaxco, K. W.; Ricci, F. *J. Am. Chem. Soc.* **2013**, *135*, 13238−13241.
(46) Modi, S.; Swetha, M. G.; Goswami, D.; Gupta, G. D.; Mayor, S.; Krishnan, Y. *Nat. Nanotechnol.* **2009**, *4*, 325−330.
(47) Saha, S.; Chakraborty, K.; Krishnan, Y. *Chem. Commun.* **2012**, *48*, 2513−2515.
(48) Hu, Y.; Cecconello, A.; Idili, A.; Ricci, F.; Willner, I. *Angew. Chem., Int. Ed.* **2017**, *56*, 15210−15233.
(49) Idili, A.; Vallée-Bélisle, A.; Ricci, F. *J. Am. Chem. Soc.* **2014**, *136*, 5836−5839.
(50) Porchetta, A.; Idili, A.; Vallée-Bélisle, A.; Ricci, F. *Nano Lett.* **2015**, *15*, 4467−4471.
(51) Ma, X.; Wang, X.; Hahn, K.; Sánchez, S. *ACS Nano* **2016**, *10*, 3597−3605.
(52) Kardash, E.; Bandemer, J.; Raz, E. *Nat. Protoc.* **2011**, *6*, 1835−1846.
(53) Howse, J. R.; Jones, R. A. L.; Ryan, A. J.; Gough, T.; Vafabakhsh, R.; Golestanian, R. *Phys. Rev. Lett.* **2007**, *99*, 8−11.
(54) Zhang, Y.; Wang, Q.; Hess, H. *ACS Catal.* **2017**, *7*, 2047−2051.
(55) Mahamdeh, M.; Schäffer, E. *Opt. Express* **2009**, *17* (19), 17190.
(56) Tolić-Nørrelykke, S. F.; Schäffer, E.; Howard, J.; Pavone, F. S.; Jülicher, F.; Flyvbjerg, H. *Rev. Sci. Instrum.* **2006**, *77* (10), 103101.
(57) Schäffer, E.; Nørrelykke, S. F.; Howard, J. *Langmuir* **2007**, *23* (7), 3654−3665.

DOI: 10.1021/acs.nanolett.8b04794
Nano Lett. 2019, 19, 3440−3447